KSME

Springer

Journal of Mechanical Science and Technology 37 (4) 2023

Original Article
DOI 10.1007/s12206-023-0322-z

Keywords:
· Tunable diode laser absorption spectroscopy
· Direct absorption spectroscopy
· Single absorption line
· Pressure measurement
· Temperature measurement

Correspondence to:
Gisu Park
gisu82@kaist.ac.kr

Citation:
Shim, H., Kim, G., Jung, S., Park, G. (2023). TDL-based spectroscopy for simultaneous measurement of multiple gas properties using a single absorption line. Journal of Mechanical Science and Technology 37 (4) (2023) 1829~1844. http://doi.org/10.1007/s12206-023-0322-z

Received June 2nd, 2022
Revised October 7th, 2022
Accepted December 15th, 2022

† Recommended by Editor Han Seo Ko

TDL-based spectroscopy for simultaneous measurement of multiple gas properties using a single absorption line

Hanseul Shim, Gyeongrok Kim, Sion Jung and Gisu Park

Department of Aerospace Engineering, Korea Advanced Institute of Science and Technology, Daejeon 34141, Korea

Abstract This study presents a single-line absorption spectroscopy method for the simultaneous measurement of gas pressure and temperature through diode laser absorption spectroscopy using a single absorption line. In the proposed method, the absorbance loss of an absorption line that may occur during baseline subtraction is predicted, and the gas properties are determined by matching a calculated absorbance to a recovered absorbance using the predicted loss. To verify the proposed method, gas property measurements are conducted for air conditions with a pressure range of 10-100 kPa and a temperature range of 300-500 K. An absorption line in the oxygen A band is selected to measure the gas properties of air. Using the proposed method, it is confirmed that the gas pressure and temperature could be measured within errors of 25 % and 18 %, respectively. When the gas pressure is predetermined using a pressure gauge, the gas temperature can be measured within an error of 14 %.

1. Introduction

Tunable diode laser absorption spectroscopy (TDLAS) is an absorption spectroscopy technique that can simultaneously measure multiple gas properties such as pressure, temperature, and concentration without direct insertion of a sensor probe. Given that TDLAS is applicable for the precise measurement of gas properties in harsh environments, it has been widely used for gas detection and diagnosis in industry and academia over the past few decades, including for gas sensing and monitoring [1-3], combustion diagnosis [4-6], gas detection in coal gasifiers [7, 8], combustion gas sensing in a piston engine [9], flow diagnosis in aerospace engines [10-13], and flow measurement in scramjet engines [14-16].

In gas diagnostics using a TDLAS system, a multiple absorption line system has been broadly used to simultaneously determine multiple gas properties. Table 1 summarizes the gas property measurement cases conducted in previous studies using laser absorption spectroscopy techniques such as direct absorption spectroscopy (DAS) and wavelength modulation spectroscopy (WMS). The number of absorption lines and the predetermined gas properties that are used to measure gas properties are also shown. As shown in Table 1, two or more absorption lines were widely used to measure multiple gas properties, whereas a single absorption line was used to measure a limited number of gas properties. In the multiple absorption line system, the gas temperature can be independently determined from an integrated absorbance ratio of two absorption lines, and the gas pressure can be determined sequentially from an integrated absorbance value using the Beer-Lambert law [17, 18]. Given that the determination procedure of gas properties is relatively simple when two or more absorption lines are used, the multiple absorption line system could be more practical than a single absorption line system.

However, installation of a TDLAS system for multiple absorption lines in a limited space, such as a transportation engine or complex industrial facility, could be difficult because additional hardware parts are required, such as diode lasers, detectors, and optical parts for different

Table 1. Gas property measurement studies using diode laser absorption spectroscopy.

Technique	Number of lines	Target gas	Predetermined property	Measured property	Ref.
DAS	2	H_2O	None	P_{H2O}, T, V	[19]
DAS	2	CO_2	P	T, X_{CO2}	[20]
DAS	>3	H_2O	P	T, X_{H2O}	[21]
DAS	4	H_2O	P	T, X_{H2O}	[22]
DAS	2	H_2O	P	T, X_{H2O}	[23]
WMS	1	CO_2	P	T, X_{CO2}	[12]
WMS	1	O_2	P, T	X_{O2}	[24]
WMS	1	O_2	P, T	X_{O2}	[25]
WMS	2	H_2O	P	T, X_{H2O}	[26]
WMS	2	H_2O	None	T	[27]
WMS	3	H_2O	P	T, X_{H2O}	[28]
WMS	3	H_2O	None	P_{H2O}, T	[29]
WMS	3	CO_2	P	T, X_{CO2}	[30]

spectral laser beams. In the multiple absorption line system, multiple diode lasers could be needed if target absorption lines are spectrally separate [11] or if absorption lines of other gas species are superposed on the target absorption line, necessitating detection of spectrally spaced absorption lines [31]. Additional optical parts, such as optical fiber couplers and diffraction gratings, could also be required to spectrally combine and separate laser beams, and multiple detectors could be essential to measure absorption lines individually. Given that the additional hardware parts occupy more space and increase the size of a TDLAS system, miniaturization is an important obstacle to overcome. In particular, the size and weight restriction of the TDLAS system are critical when installed in engines of flight vehicles such as civil aircraft and hypervelocity vehicles. In previous studies in which TDLAS systems are developed for diagnosing the airbreathing engines of hypersonic vehicles [16, 32-35], the TDLAS systems were manufactured in a size suitable for installation in flight vehicles.

In cases where a multiple absorption line system is not applicable, gas properties must be measured using a single absorption line system. If multiple gas properties such as pressure and temperature need to be measured simultaneously from a single absorption line, the gas properties could be determined from an integrated absorbance value as well as the line shape of the absorption line because no gas property can be determined individually (e.g., gas temperature). Given that the determination procedure of multiple gas properties is more straightforward in the multiple absorption line system than the single absorption line system, previous studies using a single absorption line measured only one gas property when other gas properties are predetermined, and few studies have been conducted on multiple gas property measurement, as shown in Table 1. In Benoy et al. [12], the gas temperature and concentration of carbon dioxide were simultaneously measured by detecting a single absorption line at 1997 nm using the WMS technique, which requires relatively more complicated data processing and additional parts than the DAS technique [26, 36, 37]. When multiple gas properties need to be measured using a single absorption line in a space-constrained environment, a simple absorption spectroscopy methodology using the DAS technique is required.

In this study, a single-line absorption spectroscopy method is proposed to simultaneously measure gas pressure and temperature from a single absorption line using the DAS technique, and experimental measurement of the gas properties using the proposed single-line absorption spectroscopy method is conducted. A TDLAS system is constructed using a distributed feedback (DFB) diode laser and a logarithmic amplifier to detect oxygen gas in the air. The test gas conditions are made in a gas chamber within a pressure range of approximately 10-100 kPa and temperature range of approximately 300-500 K. Gas properties for the test conditions are measured using the proposed single-line absorption spectroscopy method and compared with the actual gas properties set by the pressure gauge and the thermocouples. Validation of the proposed single-line absorption spectroscopy method is performed by comparing the gas property measurement results depending on whether the proposed single-line absorption spectroscopy method is applied. In addition, to simulate a practical case where the gas pressure is predetermined using an additional pressure sensor, gas temperature measurement is performed while the gas pressure is fixed to the set pressure measured by the Bourdon pressure gauge. Given that studies on multiple gas property measurements using a single absorption line have not been conducted extensively despite their necessity, the absorption spectroscopy method with measurement accuracy analysis presented in this study could be useful for gas property measurement in a practical environment.

2. Instruments and data processing

2.1 Laser absorption spectroscopy setup

Fig. 1 shows the TDLAS system used for absorption line detection in this study. Air is selected as the test gas. Oxygen is selected as the target gas species for gas pressure and temperature measurements because it has been used to measure the gas properties of air in laser absorption spectroscopy [13, 16, 33]. The TDLAS system is composed of four major parts: 1) laser generation parts that generate the laser beam, 2) optical parts that the laser passes through, 3) a gas chamber to make the test conditions, and 4) detection parts to detect the laser beam.

The laser generation parts that generate the laser beam are composed of a tunable diode laser, a laser driver and temperature controller to drive the diode laser, and a function generator for spectral modulation of the diode laser. To detect an absorption line of oxygen gas, a DFB diode laser with a central wavelength of 760 nm is used. A built-in collimator is installed in the diode laser so that a collimated laser beam with a diameter of

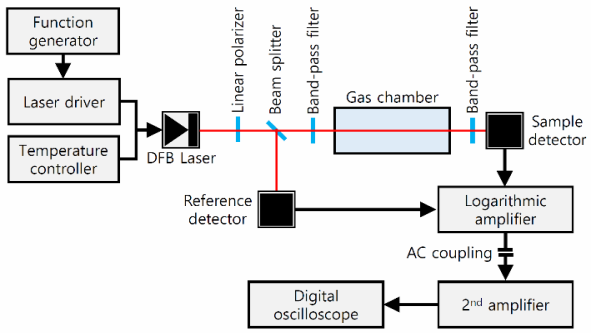

Fig. 1. Tunable diode laser absorption spectroscopy setup for oxygen absorption line detection.

approximately 1 mm is generated. The laser driver and temperature controller are designed and manufactured for the diode laser (Cosmotec, Republic of Korea) [38, 39]. Based on the modulation signal from the function generator, the laser driver supplies the current in a range of 40-110 mA to the diode laser. The temperature controller adjusts the temperature of the diode laser by controlling the built-in thermoelectric cooler in the diode laser until the temperature read from the thermistor installed in the laser is the same as a set temperature value. A function generator (model MFG 2230 M, GW Instek) is used to generate the modulation signal input to the laser driver to change the wavelength of the laser beam.

The laser beam passes through the optical parts and the gas chamber and approaches the detection parts. The optical parts are composed of a linear polarizer, a beam splitter, and band-pass filters. Given that transmissive optical components such as the beam splitter may have different optical properties such as the beam-splitting ratio depending on the polarization of the laser beam, a linear polarizer is installed in front of the diode laser. The generated laser beam is divided into a reference laser beam and a sample laser beam after the beam splitter. The reference laser beam approaches a reference detector and the sample laser beam reaches the sample detector after passing through the band-pass filters and the gas chamber. Given that any unintended stray light irradiated on the reference or sample detectors could cause distortion of the absorption line signal and errors in the gas property measurement [40], the reference detector and sample detector are installed in a closed case that blocks external light, and the band-pass filters are installed on the laser beam path to block the light of a wavelength other than the laser beam. The center wavelength of the band-pass filter is 770 nm and the full width at half maximum of the transmittance range is approximately 50 nm.

The detection parts to obtain the absorption signal are composed of the reference and sample detectors, the logarithmic amplifier, AC coupling, and a secondary amplifier. To detect the laser beam with a wavelength of 760 nm, a silicon photodiode (Model FDS1010, ThorLabs) with a measurement wavelength range of 200-1100 nm is used for the reference and sample detectors. The reference and sample detectors are reverse-biased and the generated reference and sample photocurrents are supplied into the logarithmic amplifier. Given that the logarithmic amplifier can separately amplify the absorption signal by applying the log to the ratio of the sample photocurrent and the reference photocurrent, it can be used for the DAS technique to detect a weak absorption line [41, 42]. A logarithmic amplifier for gas absorption sensing (model AD8305, Analog Devices) is used for this study. The output signal of the logarithmic amplifier V_{log} (in V) can be expressed as follows [38-40]:

$$V_{log} = G_1 \log_{10} \frac{i_{samp}}{i_{ref}} \tag{1}$$

where G_1 is the built-in gain of the logarithmic amplifier and i_{samp} and i_{ref} are the sample and reference photocurrents, respectively. To secondarily amplify the output signal of the logarithmic amplifier V_{log}, an AC coupling using a capacitor is applied after the logarithmic amplifier to reduce noise in the output signal and remove potential DC offset [38, 39, 41]. To make the absorption signal measurable, the signal after AC coupling is secondarily amplified using a secondary amplifier. The raw signal V_{meas} after AC coupling and the secondary amplifier is expressed as follows [38, 39]:

$$V_{meas} = G_2 \left(G_1 \log_{10} \frac{i_{samp}}{i_{ref}} + V_{adjust} \right) \tag{2}$$

where G_2 is the gain of the secondary amplifier and V_{adjust} is the adjusted voltage value in the measurement caused by the AC coupling. If the raw signal V_{meas} is measured instantaneously when the test gas condition is stable, V_{adjust} could be assumed to be constant during the measurement time [38, 39]. Because the photocurrent of the reverse-biased silicon photodiode is linearly proportional to the irradiated light intensity, Eq. (2) can be expressed as follows:

$$V_{meas} = G_{tot} \log_{10} \frac{I_{samp}}{I_{ref}} + C_{arbi} \tag{3}$$

where G_{tot} is the total gain obtained by multiplying the built-in gain of the logarithmic amplifier G_1 and that of the secondary amplifier G_2, and I_{samp} and I_{ref} are the intensity of the laser beam irradiated to the sample and reference photodiode, respectively. When a laser beam with a path length of approximately 28 cm passes through the gas chamber filled with room-temperature air with pressure below 1 atm, the intensity of the sample laser beam could be attenuated to less than 1 % by the oxygen gas [38, 39]. Considering the intensity attenuation of the sample laser beam, the total gain G_{tot} is set to 62 to make the absorption line signal in the raw signal a voltage level of a few hundred millivolts, which is a sufficient voltage for measurement using an oscilloscope. A digital oscilloscope (model GDS-1074B, GW Instek) with eight bits of vertical resolution is used for measurement of the raw signal V_{meas}.

2.2 Laser modulation

A laser beam generated from a DFB diode laser can be spectrally modulated by changing the applied current or temperature of the laser diode [43]. For a DFB diode laser, a larger spectral modulation range can be achieved with temperature control than with applied current control; however, the spectral modulation speed is much slower in temperature control [43]. In this study, spectral modulation is performed using the applied current control to detect a target absorption line, and the median spectral position of the modulation range is adjusted by the temperature control. A ramp-shaped spectral laser modulation is adopted since it has been widely used for laser absorption spectroscopy [19, 31, 44] because of the advantage that the wavenumber can be modulated linearly with time. A ramp-shaped modulation signal with a frequency of 5 kHz is generated from the function generator to linearly change the wavenumber of the laser.

2.3 Time-to-wavenumber conversion

To compare the temporal raw signal $V_{meas}(t)$ measured using the oscilloscope with the calculated absorbance $A_{calc}(v)$ where v is the wavenumber (in cm^{-1}), axis conversion is conducted in two steps: 1) time-to-wavenumber conversion to convert the temporal raw signal $V_{meas}(t)$ to the spectral raw signal $V_{meas}(v)$ and 2) Y-axis conversion to convert the spectral raw signal to the measured absorbance $A_{calc}(v)$.

In the time-to-wavenumber conversion, temporal change data for the absolute wavenumber are obtained using temporal change data for the relative wavenumber measured using an unbalanced interferometry setup and the temporal position of the absolute wavenumber value of an absorption line detected using the TDLAS setup shown in Fig. 1. Fig. 2 shows an unbalanced interferometry setup to measure the temporal change data for the relative wavenumber. Given that the temporal change in the laser wavenumber depends on the modulation frequency [45], the temporal change data for the absolute wavenumber must be experimentally measured. To convert the temporal raw signal $V_{meas}(t)$ to the spectral raw signal $V_{meas}(v)$ considering the variable spectral modulation characteristics of the DFB diode laser, the temporal change of the wavenumber is experimentally measured. Although a solid etalon has been broadly used to measure the temporal change of the wavenumber [44, 46, 47], the unbalanced interferometry setup that can produce a longer path difference than a solid etalon is utilized to increase the spectral resolution of temporal wavenumber change measurement. The unbalanced interferometry setup shown in Fig. 2 adopts a Mach-Zehnder configuration that uses the interferometric phenomenon that occurs when two laser beams with different path lengths are simultaneously irradiated to a photodetector [48]. As shown in Fig. 2, the laser beam starting from a diode laser is divided into two laser beam paths after the first beam splitter. One laser beam passes through the second beam splitter and reaches the photodetector, while the other laser beam which is reflected at the first beam splitter travels a longer distance through the mirrors before reaching the photodetector. The beam splitters and the mirrors are separated by a distance of L_{intf} which is half of the path difference between the two laser beams. A variable neutral density (ND) filter is installed on one laser beam to obtain an optimal interferometry signal by adjusting the laser beam intensity.

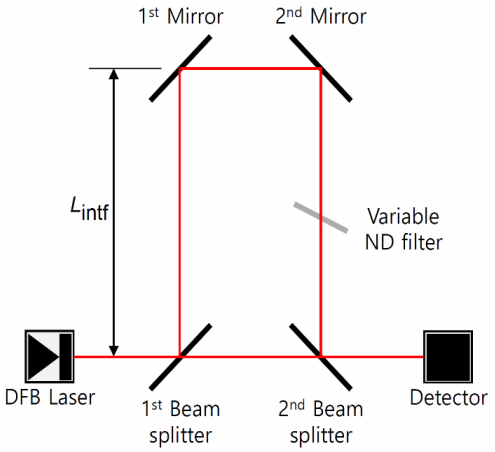

Fig. 2. Unbalanced interferometry setup for temporal wavenumber change measurement [39].

When the spectrally modulated laser is measured using the unbalanced interferometry setup shown in Fig. 2, an interferometry signal $V_{intf}(t)$ that has a sinusoidal waveform can be detected [48]. The interval between two adjacent peaks of the measured interferometry signal has a constant wavenumber called the free spectral range (FSR). The FSR (in Hz) is determined by the path length difference between the two laser beams in the interferometry setup, and can be expressed as follows [44]:

$$\mathrm{FSR}=\frac{c}{2nL_{intf}} \tag{4}$$

where c is the speed of light and n is the refractive index of air. Based on the relation between the frequency and wavenumber of light, the FSR (in cm^{-1}) can be calculated by dividing the FSR (in Hz) by the speed of light.

When the wavenumber of the laser changes over time, a peak is observed in the interferometry signal $V_{intf}(t)$ whenever the wavenumber of the laser changes by the FSR. If the FSR is much smaller than the spectral modulation range, several peaks with different temporal positions can be observed in an interferometry signal. Using the temporal position of the peaks in the interferometry signal $V_{intf}(t)$, temporal change data of the relative wavenumber are obtained. After obtaining the temporal relative wavenumber change data, the temporal position of the absolute wavenumber value is obtained from the detected absorption line in the temporal raw signal $V_{meas}(t)$. Using the obtained temporal change data of the relative wavenumber

and the temporal position of the absolute wavenumber value, temporal change data of the absolute wavenumber are calculated.

2.4 Y-axis conversion

In the Y-axis conversion, the spectral raw signal $V_{meas}(v)$ is converted to the measured absorbance $A_{meas}(v)$ to compare the measured absorption signal with the calculated absorbance. The intensities of the laser beams irradiated to the sample detector and reference detector can be expressed as follows [38-40]:

$$\begin{cases} I_{samp}(\nu)=\tau_{bs}I_0(\nu)\tau_{optic}\exp\left(-A_{meas}(\nu)\right) \\ I_{ref}(\nu)=\left(\tau_{bs}-1\right)I_0(\nu) \end{cases} \quad (5)$$

where $I_0(v)$ is the intensity of the laser beam generated by the diode laser, τ_{bs} is the transmittance of the beam splitter, τ_{optic} is the total transmittance of the optical components that the sample laser beam passes, and $A_{meas}(v)$ is the absorbance of the absorption line. If the spectral modulation range of the laser is narrow so that the spectral sensitivities of the optical parts used in the TDLAS setup can be assumed to have a constant value within the spectral modulation range, a constant can be defined as follows [38, 39]:

$$C_3=\frac{r-1}{r\tau_{optic}}. \quad (6)$$

By substituting Eqs. (5) and (6) into Eq. (3), the spectral raw signal $V_{meas}(v)$ can be expressed as follows [38]:

$$V_{meas}(\nu)=G_{tot}\log_{10}\left(\frac{\exp\left(-A_{meas}(\nu)\right)}{C_3}\right)+C_{arbi}. \quad (7)$$

If the gas chamber is fully evacuated so that the target gas is absent, the absorbance of the absorption line $A_{meas}(v)$ is zero. When the absorbance of the absorption line is zero, the spectral raw signal with an absence of the absorption line becomes a baseline for the raw signal. The baseline for the spectral raw signal $V_{bl,meas}(v)$ can be expressed as follows:

$$V_{bl,meas}(\nu)=-G_{tot}\log_{10}C_3+C_{arbi}. \quad (8)$$

If the baseline is determined, the absorbance of an absorption line can be extracted by subtracting the baseline from the spectral raw signal. The extracted absorbance can be expressed as follows:

$$A_{meas}(\nu)=-\ln\left[10^{\left(\frac{V_{meas}(\nu)-V_{bl,meas}(\nu)}{G_{tot}}\right)}\right]. \quad (9)$$

The spectral absorbance of the target absorption line can be determined using Eq. (9) from the measured spectral raw signal $V_{meas}(v)$ when the baseline $V_{bl,meas}(v)$ is determined.

3. Single-line absorption spectroscopy method

3.1 Absorption spectroscopy

When a laser beam passes through the test gas, the laser beam intensity after the test gas is calculated using Beer–Lambert's law as follows [18]:

$$I_{af}(\nu)=I_{bf}(\nu)\exp\left(-k(\nu)L\right) \quad (10)$$

where $I_{bf}(v)$ and $I_{af}(v)$ are the intensity of the laser beam before and after the test gas, respectively, $k(v)$ is the spectral absorption coefficient, and L is the laser beam path length in the test gas. The spectral absorbance $A(v)$, which is the product of the spectral absorption coefficient and the laser beam path length, can be expressed as follows [18]:

$$A(\nu)=k(\nu)L=S(T)\phi(\nu)PX_iL \quad (11)$$

where $S(T)$ (in $cm^{-2}atm^{-1}$) is the line strength of the absorption line at gas temperature T (in K), $\phi(v)$ (in cm) is the line shape function, P (in atm) is the gas pressure, and X_i is the mole fraction of the target gas species in the test gas. As shown in Eq. (11), the spectral absorbance is a function of the gas pressure and temperature of the test gas, the mole fraction of the target gas species, and the beam path length. The line strength $S(T)$ can be expressed as follows [18]:

$$S(T)=S(T_0)\frac{Q(T_0)}{Q(T)}\left(\frac{T_0}{T}\right)\exp\left[-\frac{hcE''}{k_B}\left(\frac{1}{T}-\frac{1}{T_0}\right)\right] \quad (12)$$

where $S(T_0)$ is the line strength at reference temperature T_0, $Q(T)$ is the partition function of the target gas species, h is the Planck constant, k_B is the Boltzmann constant, and E'' is the lower state energy of the transition.

The line shape function $\phi(v)$ characterizes the absorbance distribution of an absorption line with respect to the wavenumber considering the broadening mechanism. When the energy levels of a transition are perturbed due to physical processes such as collisions between the molecule in the gas, line shape broadening of the corresponding absorption line occurs. The commonly used line shape functions are the Lorentzian profile and the Gaussian profile, which are induced by the collisional process between the molecules and the thermal movement of the molecule, respectively. Given that the collision and thermal movement of the molecules occur simultaneously in the common case [18], the Voigt profile, which is a convolution of the Lorentzian and Gaussian profiles, is widely used. The Voigt profile is a function of the pressure and temperature of the test gas and the mole fraction of the target gas species [18].

The integration of the line shape function over the wavenumber is unity:

$$\int_{-\infty}^{\infty}\phi(\nu)d\nu=1\,. \tag{13}$$

From Eqs. (12) and (13), the integrated absorbance A can be calculated as follows:

$$A(\nu)=\int_{-\infty}^{\infty}A(\nu)d\nu=S(T)PX_iL\,. \tag{14}$$

As shown in Eq. (14), the integrated absorbance is a function of the pressure and temperature of the test gas and the mole fraction of the target gas species.

3.2 Gas property determination with line shape recovery

In the multiple absorption line system that detects two or more absorption lines, gas pressure and temperature can be determined simultaneously using the measured integrated absorbances of the absorption lines. Given that the ratio of the integrated absorbances of different absorption lines is a function of temperature, the gas temperature can be determined independently regardless of the gas pressure or mole fraction using the ratio of the integrated absorbance. When the beam path length is known, the partial pressure of the target gas species can be determined from the determined gas temperature using Eq. (14). If the mole fraction of the target gas species is fixed, such as the oxygen in the air, the gas pressure of the test gas can be obtained from the partial pressure.

Unlike the multiple absorption line system, the ratio of the integrated absorption cannot be obtained in the single absorption line system so a different procedure is required to simultaneously determine the gas pressure and temperature. Given that the line shape of an absorption line is a function of the gas pressure and temperature, the gas properties can be determined by line fitting the calculated line shape function to the measured absorption line signal. When the gas properties are determined through line shape fitting, measurement of the absorption line without any distortion or loss is important because the line shape is affected by pressure and temperature.

Fig. 3 shows examples of Gaussian and Lorentzian profiles with a Doppler linewidth $\Delta\nu_D$ of 0.04 cm^{-1} and the same collisional linewidth $\Delta\nu_L$. The white region in Fig. 3 represents a central region near the absorption line center and the shaded region represents a wing region far from the line center. As shown in Fig. 3, the Gaussian profile has a higher absorption amplitude than the Lorentzian profile in the central region, while the Lorentzian profile has a higher absorption amplitude in the wing region. Given that the Lorentzian profile is strongly affected by the gas pressure and the Gaussian profile is a function of the gas temperature, the spectral absorbance in the central region could be more affected by gas temperature than by pressure. In the wing region, because the Lorentzian profile has a much higher absorbance than the Gaussian profile, the spectral absorbance could be determined predominantly by the gas pressure. The spectral absorbance in the wing region of the Voigt profile, which is a convolution of the Gaussian and Lorentzian profiles, could also be affected by the gas pressure.

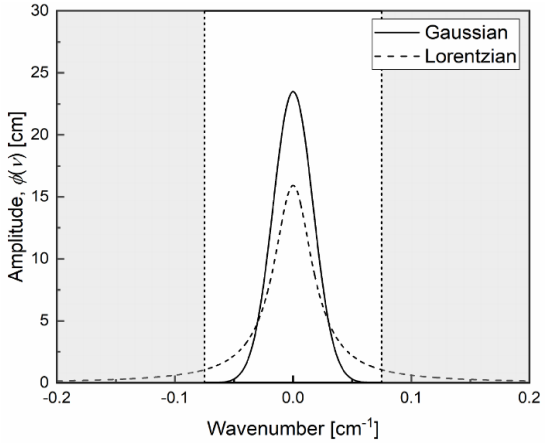

Fig. 3. Calculated gaussian and lorentzian line shape function for $\Delta\nu_D = \Delta\nu_L$ = 0.04 cm^{-1} with central region (white) and wing region (gray).

Given that the influence of gas properties on the line shape differs in the central and wing regions, the absorption line needs to be measured without loss of absorbance in the central and wing regions to precisely determine the gas pressure and temperature. However, absorbance loss of the measured absorption line could occur during the baseline subtraction if the baseline $V_{bl,meas}(\nu)$ is determined using the wing region shown in Fig. 3. The measured absorbance after the baseline subtraction could be near zero, especially in the wing region. When line fitting is conducted between the calculated line shape function and the measured absorbance at which the absorbance loss occurs, the gas properties are incorrectly determined, and a large error can occur in the gas pressure determination.

To detect the absorption line without distortion, studies on methodologies for accurate baseline determination or absorption line correction have been conducted [39, 49-51]. Given that the proposed methodology for a precise measurement of the absorption line can be used for the multiple absorption line system [51] or verified for concentration measurement [49, 50], a new methodology is needed to measure multiple gas properties using a single absorption line. In this study, a single-line absorption spectroscopy method is proposed to measure multiple gas properties from a single absorption line by recovering the line shape of the measured absorption line using a procedure to predict the absorbance loss of the measured absorbance $A_{meas}(\nu)$.

Fig. 4 shows a flow chart of the proposed single-line absorption spectroscopy method to measure gas pressure and temperature. The single-line absorption spectroscopy method is performed through the following steps:

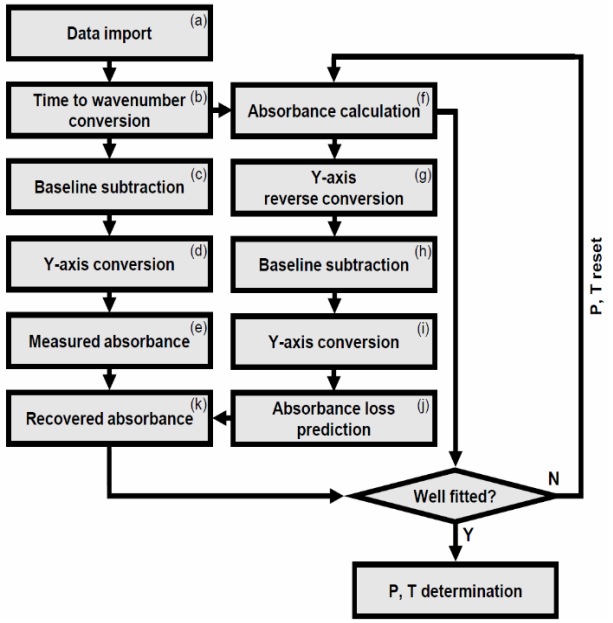

Fig. 4. Flow chart for the proposed single-line absorption spectroscopy method [39].

a) Input data such as the temporal raw signal $V_{meas}(t)$, the spectroscopic parameters of the target absorption line, and the initial values of gas pressure and temperature for the iteration are imported. The spectroscopic parameters are the center wavenumber ν_0, the line strength at reference temperature $S(T_0)$, the lower state energy of the transition E'', the air-broadened half width at half maximum (HWHM) at reference temperature γ_{air}, the self-broadened HWHM at reference temperature γ_{self}, and the coefficient of the temperature dependence of the air-broadened half width n_{air}. The spectroscopic parameters are obtained from the HITRAN2016 database [52]. The initial values of the gas pressure and temperature are set to the median of the target pressure and temperature ranges of the test gas.

b) Time to wavenumber conversion is conducted to convert the temporal raw signal $V_{meas}(t)$ to the spectral raw signal $V_{meas}(\nu)$.

c) Baseline subtraction is conducted to subtract the baseline $V_{bl,meas}(\nu)$ determined in the spectral raw signal from the spectral raw signal $V_{meas}(\nu)$. Using the concept of a wing level threshold introduced in Sec. 3.3, the boundary between the central and wing regions of the absorption line is determined. The baseline $V_{bl,meas}(\nu)$ is determined by fitting a fourth-order polynomial function to the wing region of the absorption line.

d), e) Y-axis conversion is conducted using Eq. (9) to convert the baseline-subtracted spectral raw signal to the measured absorbance $A_{meas}(\nu)$.

f) The calculated absorbance $A_{calc}(\nu)$ for the spectral modulation range obtained in step (b) is computed using Eq. (11) at the gas pressure and temperature of the current iteration. The mole fraction is fixed at 0.21 because the concentration of oxygen in the air is constant. The Voigt profile is calculated using the algorithm proposed in the work of Abrarov et al. [53] and used as the line shape function $\phi(\nu)$.

In a basic DAS technique, the measured absorbance $A_{meas}(\nu)$ obtained in step (e) is directly compared with the calculated absorbance $A_{calc}(\nu)$ obtained in step (f). In this study, additional steps are performed to predict the measured absorbance loss that could occur during the baseline subtraction in step (c). The additional steps also entail baseline subtraction for the calculated absorbance and prediction of the absorbance loss by calculating the difference between the calculated absorbance and the baseline-subtracted calculated absorbance. The additional steps for prediction of the absorbance loss are as follows:

g) Y-axis reverse conversion is conducted to obtain the calculated signal $V_{calc}(\nu)$ from the calculated absorbance $A_{calc}(\nu)$ obtained in step (f) to perform the baseline subtraction for a signal in voltage units, similar to the spectral raw signal $V_{meas}(\nu)$. Because the calculated signal $V_{calc}(\nu)$ does not have a baseline, the equation for the Y-axis reverse conversion is obtained by rearranging Eq. (9) for the zero baseline and can be expressed as follows:

$$\mathrm{V_{calc}}(\nu)=\mathrm{G_{tot}}\log_{10}\left[\exp\left(-\mathrm{A_{calc}}(\nu)\right)\right]. \tag{15}$$

h) The baseline $V_{bl,calc}(\nu)$ is computed and subtracted from the calculated signal $V_{calc}(\nu)$ in the same manner as in step (c) to obtain a baseline-subtracted calculated signal.

i) The baseline-subtracted calculated signal is Y-axis converted. Using Eq. (9), the baseline-subtracted calculated absorbance is calculated from the calculated signal $V_{calc}(\nu)$ and baseline $V_{bl,calc}(\nu)$ in the same way as in step (d).

j) The predicted absorbance loss $A_{loss,pred}(\nu)$ is calculated by subtracting the baseline-subtracted calculated absorbance from the calculated absorbance. Given that the actual absorbance loss $A_{loss,actual}(\nu)$ that occurred during steps (a) to (f) cannot be experimentally measured, the predicted absorbance loss $A_{loss,pred}(\nu)$ is used to recover the measured absorbance $A_{meas}(\nu)$.

k) The recovered absorbance $A_{meas,recov}(\nu)$ is obtained by adding the predicted absorbance loss $A_{loss,pred}(\nu)$ to the measured absorbance $A_{meas}(\nu)$. The recovered absorbance is compared with the calculated absorbance $A_{calc}(\nu)$.

Iteration of steps (c) to (k) is performed by changing the gas pressure and temperature until the root mean square error (RMSE) between the recovered absorbance $A_{meas,recov}(\nu)$ and the calculated absorbance $A_{calc}(\nu)$ is minimized and converged. After the termination of the iteration, the gas pressure and temperature of the final iteration are used as the measured gas pressure P_{meas} and temperature T_{meas}, respectively.

Fig. 5 shows a running example of the flow chart shown in Fig. 4 for a temporal raw signal sample. As shown in Fig. 5, the absorbance loss induced by the baseline subtraction is successfully predicted, so that the predicted absorbance loss is well-matched with the actual absorbance loss. Consequently,

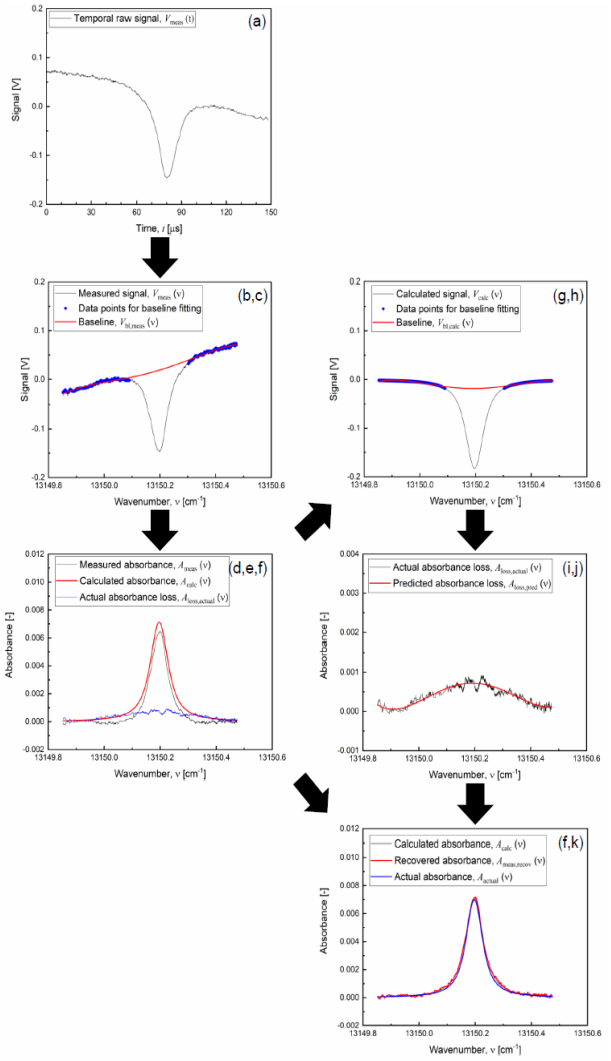

Fig. 5. Proposed procedure of gas pressure and temperature determination with line shape recovery for a measured absorption data sample [39].

the measured absorbance could be recovered successfully by using the proposed single-line absorption spectroscopy method.

3.3 Wing level threshold

Fig. 6 shows an example of determining a central region and a wing region using a wing level threshold that is conducted in steps (c) and (h) in the proposed single-line absorption spectroscopy method. The wing level threshold is a value expressed as a percentage and is used as a criterion to determine the boundary wavenumber value dividing the central and wing regions. The wavenumber value of the boundary is determined when the spectral absorbance of the absorption line is equal to an absorbance value calculated by multiplying the maximum absorbance value of the absorption line by the wing level threshold. As shown in Fig. 6, two boundaries can be determined in an absorption line; one has a higher wavenumber value than the center wavenumber of the absorption line and the other has a lower wavenumber value.

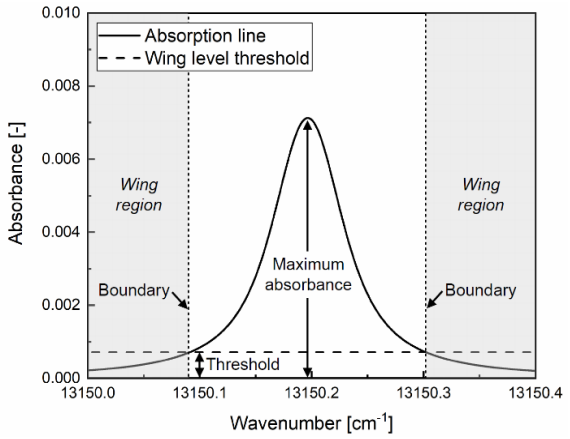

Fig. 6. Wing region decision using a wing level threshold for an absorption line [39].

The wing level threshold is determined from the calculated absorbance in step (f) and used for steps (c) and (h) in the flow chart. During the iterative process, a wing level threshold value determined in step (f) is used for steps (c) and (h) in the same iteration and is newly determined when a new iteration proceeds.

4. Test conditions and gas property measurement

To verify that the gas pressure and temperature can be measured using the proposed single-line absorption spectroscopy method, test conditions with a pressure range of approximately 10-100 kPa and temperature range of approximately 300-500 K are created in a gas chamber and the gas properties of the test conditions are measured.

4.1 Gas chamber

Fig. 7 shows a schematic and pictures of the gas chamber for test condition generation. Fig. 7(a) shows a schematic of the gas chamber, Fig. 7(b) shows an exterior photograph of the gas chamber with measurement instruments, and Fig. 7(c) shows an interior photograph of the gas chamber during heating. The gas chamber is rectangular, with a height of 40 mm, and is made of stainless steel. Pipelines are installed on the gas chamber to connect the gas chamber with a vacuum pump and a Bourdon pressure gauge. A vent line is installed on the gas chamber for ventilation. The vacuum pump is used to evacuate the gas chamber. The gas pressure of the test condition is adjusted to the desired pressure value P_{set} using the Bourdon pressure gauge.

An electrical heating method is adopted to heat the test gas above room temperature. A resistance heating wire (Kanthal A-1, Kanthal) is installed by being wound along the inner wall of the gas chamber. The resistance of the wire is approximately

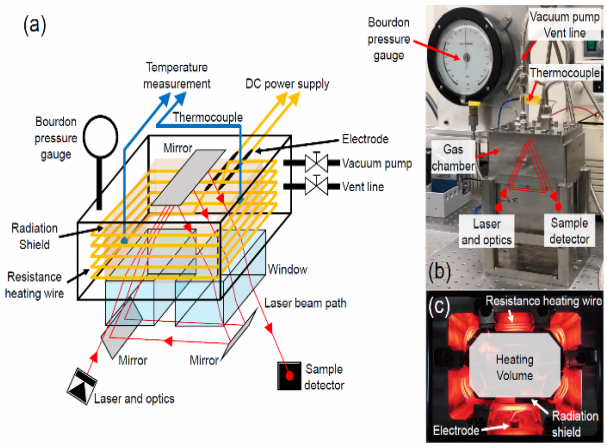

Fig. 7. A schematic and pictures of the gas chamber for pressure and temperature measurements: (a) a schematic of the gas chamber; (b) a picture of the gas chamber with laser and optics installation; (c) inner structure picture of the gas chamber during heating [39].

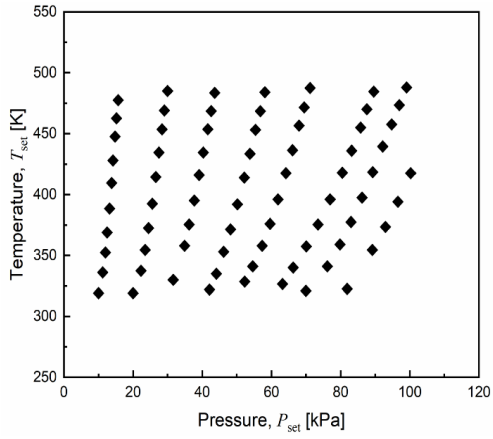

Fig. 8. Test conditions for gas pressure and temperature measurements [39].

4.8 Ω. Two electrodes are installed through the gas chamber to supply the electrical power to the resistance heating wire from an electrical power source outside of the gas chamber. A DC power supply (model EX80-22.5TB, ODA Technologies) is used as the electrical power source to supply up to 370 W of power to the resistance heating wire. Two K-type thermocouples are installed in the gas chamber to measure the test gas temperature. A brass radiation shield in the shape of a thin plate is installed in the gas chamber to spatially separate the heating volume from the resistance heating wire as shown in Figs. 7(a) and (c). The radiation shield prevents the thermocouple's junction beads from being exposed to the surface radiation of the resistive heating wire, allowing for the thermocouple to measure the gas temperature without radiative disturbance by the resistive heating wire. The set temperature T_{set} of the test condition is set using the thermocouples.

The diode laser, the optical parts such as the linear polarizer, beam splitter, band-pass filter, and the reference and sample detectors are installed outside of the gas chamber. At the bottom of the gas chamber, two optical windows made of sapphire are installed for the optical access of the laser beam. A triangular spiral-shaped laser beam path configuration is constructed in the gas chamber as shown in Fig. 7 to maximize the signal-to-noise ratio (SNR). By applying the triangular spiral-shaped laser beam path, the spectral absorbance can be amplified by increasing laser beam path length inside the gas chamber and the etalon effect due to reflection on both sides of the optical window could be significantly reduced by passing the laser beam obliquely through the optical window. One internal mirror installed at the inner wall of the gas chamber and two external mirrors installed outside the gas chamber are used to make the laser beam pass through the gas chamber three times in a triangular shape. After propagating three times in the gas chamber, the laser beam reaches the sample detector. The two sides of the triangular laser beam path are inside the gas chamber while the other side is outside. Given that the absorption line measurement in the gas chamber could be disturbed by laser absorption in the external laser beam path, the laser absorption by the gas outside the gas chamber is minimized by placing the external side of the triangular laser beam path in a vacuum. To make the laser beam path an equilateral triangle shape, the external mirrors are tilted at an angle of 30 degrees and the laser beam enters the gas chamber with an angle of incidence of 30 degrees, as shown in Fig. 7. The total laser beam path length passing through the test gas inside the gas chamber is approximately 28 cm [38, 39].

4.2 Test conditions

Fig. 8 shows the test conditions within a pressure range of approximately 10-100 kPa and temperature range of approximately 300-500 K in the gas chamber. A pressure range of approximately 10-100 kPa and temperature range of approximately 300-500 K are selected as the target gas property region for gas property measurements using the proposed single-line absorption spectroscopy method. The diamond symbols in Fig. 8 are the 74 test conditions generated in the gas chamber. As shown in Fig. 8, the test conditions cover the target gas property region for gas pressure and temperature measurement.

Before generating the test conditions, the gas chamber is evacuated using a vacuum pump. After evacuation, the gas chamber is filled with air to the desired initial pressure using the Bourdon pressure gauge. Then, all pipelines except the Bourdon pressure gauge are closed to prevent test gas leakage and convection heat transfer. The test gas is heated by supplying constant electrical power to the resistance heating wire from the DC power supply. The gas temperature is monitored using thermocouples until it reaches a steady state. When the test conditions are maintained with steady pressure and temperature, the gas pressure and the temperature are measured using the Bourdon pressure gauge and thermocouples, respectively, and the temporal raw signal $V_{meas}(t)$ is recorded using the oscilloscope. The gas temperature is obtained by

averaging the measured temperatures from the thermocouples. The test gas in the gas chamber is assumed to have a uniform temperature because the measured temperatures have a temperature deviation within 3 %. The test condition generation procedure is repeated for the initial pressure range of 10-80 kPa and electrical power range of 0-350 W so that the gas pressures and temperatures of the test conditions can cover the target gas property region. For all test conditions, the wavenumber modulation and temperature control of the diode laser are maintained to consistently measure the temporal raw signal $V_{meas}(t)$.

4.3 Absorption line selection

Laser absorption spectroscopy for air can be performed using absorption lines in the oxygen *A* band in the wavenumber range of 12987-13175 cm^{-1} [54, 55]. To measure the gas pressure and temperature using the proposed single-line absorption spectroscopy method, a target absorption line is selected in the oxygen *A* band based on the following criteria. 1) To apply the proposed single-line absorption spectroscopy method on an independent absorption line, absorption lines that are not superimposed by another strong absorption line are selected. 2) To achieve a high SNR on the absorption line measurement for the test conditions at room temperature, strong absorption lines with a line strength at reference temperature $S(T_0)$ above 1.0×10^{-4} $cm^{-2}atm^{-1}$ are considered. 3) To ensure a high SNR on the absorption line measurement for the high-temperature test conditions, absorption lines that have a high lower state energy *E"* are considered. The line strength of an absorption line with a high lower state energy does not significantly weaken under high-temperature gas conditions, as can be observed in Eq. (12). 4) Considering the wavenumber modulation limitation of the diode laser used in this study, absorption lines within a wavenumber range of 13140-13157 cm^{-1} are considered. Based on the criteria for the selection of a target absorption line, the absorption line at 13150.2 cm^{-1} is selected as the target absorption line.

4.4 Wing level threshold determination and gas property measurement

The wing level threshold is determined prior to the measurement of gas properties to achieve maximum accuracy in gas property measurement. A tendency of the gas property measurement accuracy with respect to the wing level threshold is observed through the simulation and the experimental measurement to determine the wing level threshold.

In the simulation, a calculated signal $V_{calc}(v)$ that the Y-axis reverse-converted from a calculated absorbance $A_{calc}(v)$ is used instead of the spectral raw signal $V_{meas}(v)$ in step (b) in the flow chart. For several simulation gas pressures and temperatures in the target gas property region, the gas pressures and temperatures are determined using the proposed single-line absorption spectroscopy method, and the gas property measurement accuracy for simulation is obtained from the difference between the simulation gas properties and the determined gas properties. In the experimental measurement, the gas property measurement accuracy is obtained from the set gas properties of the test conditions shown in Fig. 5 and the determined gas properties using the single-line absorption spectroscopy method. The simulation and the experimental measurement are conducted repeatedly for various wing level threshold values. The wing level threshold is determined at the maximum accuracy.

Using the determined wing level threshold, the gas pressure and temperature for the test conditions are measured using the single-line absorption spectroscopy method. The measured gas pressure and temperature are compared with the set gas pressure and temperature, respectively.

5. Results and discussion

5.1 Time-to-wavenumber conversion

Fig. 9 shows the time-to-wavenumber conversion results of the temporal raw signal $V_{meas}(t)$ using the unbalanced interferometry setup. The measured interferometry signal $V_{intf}(t)$ with detected peaks is shown in Fig. 9(a). The spectral interval between the two adjacent peaks is the FSR. To obtain sufficient spectral resolution for the time-to-wavenumber conversion, the FSR is adjusted to 0.025 cm^{-1} by setting the distance between

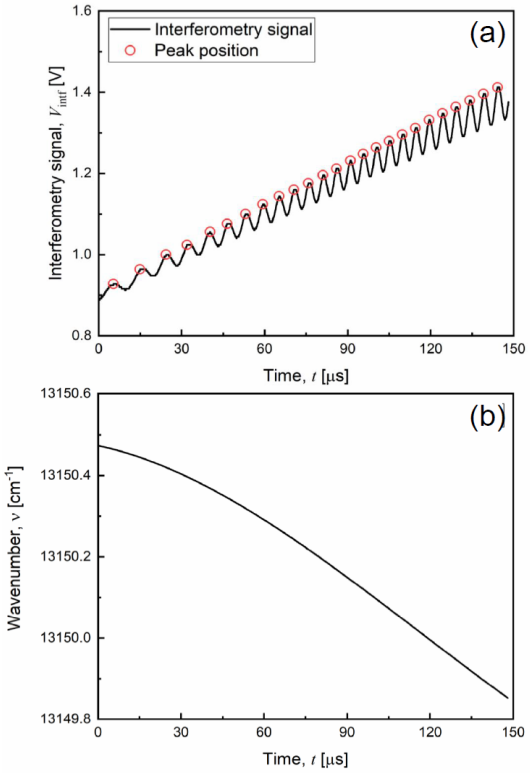

Fig. 9. Time to wavenumber conversion results: (a) measured interferometry signal; (b) determined temporal wavenumber change [39].

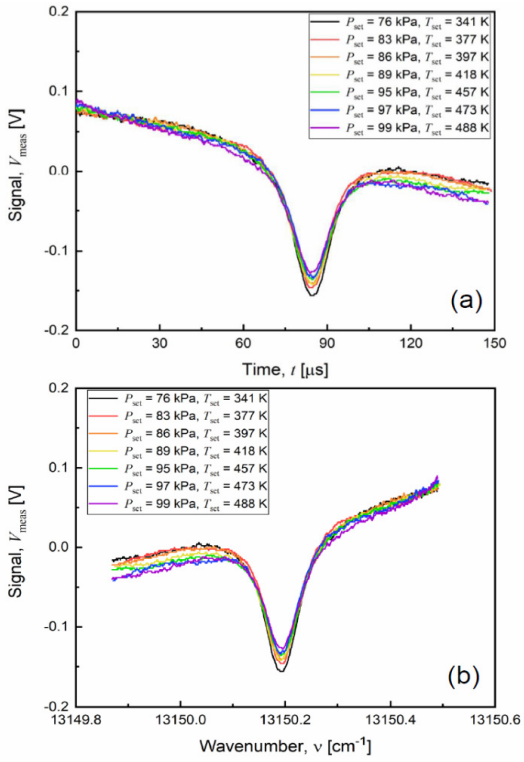

Fig. 10. Measured raw signal for several test conditions: (a) measured temporal raw signal; (b) measured spectral raw signal [39].

the beam splitters and mirrors L_{intf} to 20 cm. The temporal change data of the relative wavenumber are obtained from the temporal positions of the detected peaks. Fig. 9(b) shows the temporal absolute wavenumber change of the laser beam calculated from the temporal change data of the relative wavenumber and the temporal position of the target absorption line. As shown in Fig. 9(b), the wavenumber of the laser beam decreases linearly over time within 50-150 μs. Using the wavenumber change data shown in Fig. 9(b), the temporal raw signal $V_{meas}(t)$ is converted to the spectral raw signal $V_{meas}(v)$.

5.2 Measured absorption lines

Fig. 10 shows the temporal raw signal $V_{meas}(t)$ measured in several test conditions within a pressure range of 70-100 kPa and temperature range of 300-500 K, and the spectral raw signal $V_{meas}(v)$ after the time-to-wavenumber conversion. To increase the SNR, the temporal raw signal $V_{meas}(t)$ is obtained by averaging 256 data. As shown in Fig. 10, the absorbance of the central region in the target absorption line decreases as the gas pressure and temperature increase because the line strength becomes weaker as the temperature increases and the line broadening becomes stronger.

5.3 Wing level threshold determination

The wing level threshold is determined within a range of

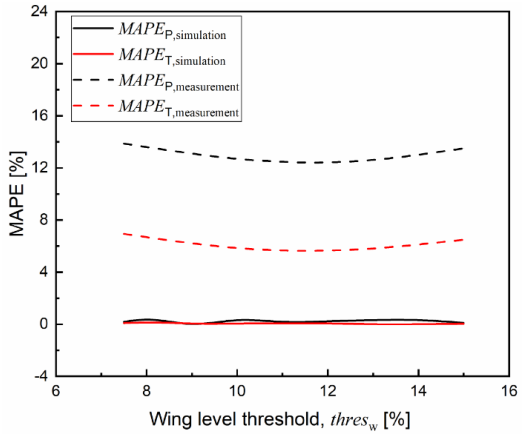

Fig. 11. Simulated and experimentally measured results of the gas pressure and temperature accuracy for different wing level thresholds [39].

7.5 %-15 % through the simulation and experimental measurement of the gas property measurement accuracy. A mean absolute percentage error (MAPE) is used to examine the gas property measurement accuracy. The MAPE is computed for the gas pressure and temperature separately to observe the dependence of the measurement accuracy on the gas pressure and temperature individually.

In the simulation, the calculated signals $V_{calc}(v)$ are computed for a pressure range of 10-100 kPa and temperature range of 300-500 K with a pressure interval of 10 kPa and a temperature interval of 25 K and used instead of the measured spectral signal $V_{meas}(v)$. The gas pressures and temperatures are determined using the proposed single-line absorption spectroscopy method for the calculated signals, and the MAPE for simulation $MAPE_{simulation}$ is computed using the simulation gas properties and determined gas properties. In the experimental measurement, the MAPE for experimental measurement $MAPE_{measurement}$ is computed using the set gas properties and the measured gas properties from the spectral raw signal $V_{meas}(v)$.

Fig. 11 shows a comparison between the simulated and the experimentally measured gas property measurement accuracies for the considered range of the wing level threshold. Black and red colors represent the gas property measurement accuracy for gas pressure and temperature, respectively, and the solid and dashed lines represent the simulation and experimental measurements, respectively. As shown in Fig. 11, the gas property measurement accuracy is low for the gas pressure and temperature in the simulation results. The maximum MAPE values of the simulation for gas pressure and temperature are 0.4 and 0.2 %, respectively. On the other hand, the experimentally measured MAPE values for gas pressure and temperature are 15 and 5.7 %, respectively, which are higher than the simulation. Although the simulation predicts a nearly constant measurement accuracy, the experimental measurement predicts that the maximum gas property measurement accuracy can be achieved when the wing level threshold is between 10 and 12. A possible reason for the difference in the

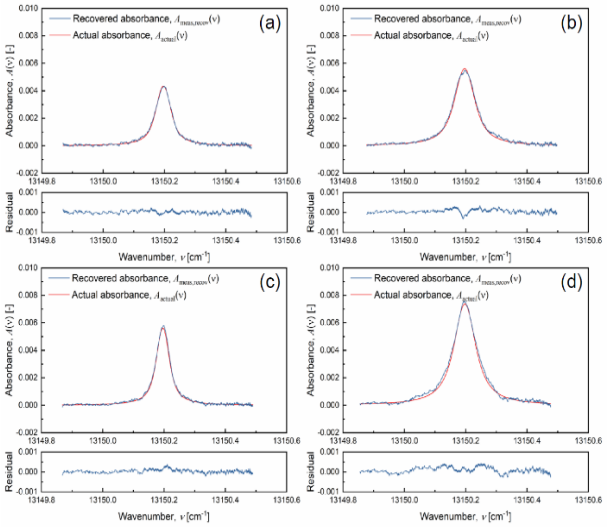

Fig. 12. Comparison between the recovered absorbance $A_{meas,recov}(v)$ and the actual absorbance $A_{actual}(v)$ for several test conditions: (a) P_{set} = 44 kPa, T_{set} = 483 K; (b) P_{set} = 88 kPa, T_{set} = 470 K; (c) P_{set} = 32 kPa, T_{set} = 330 K; (d) P_{set} = 82kPa, T_{set} = 322 K [39].

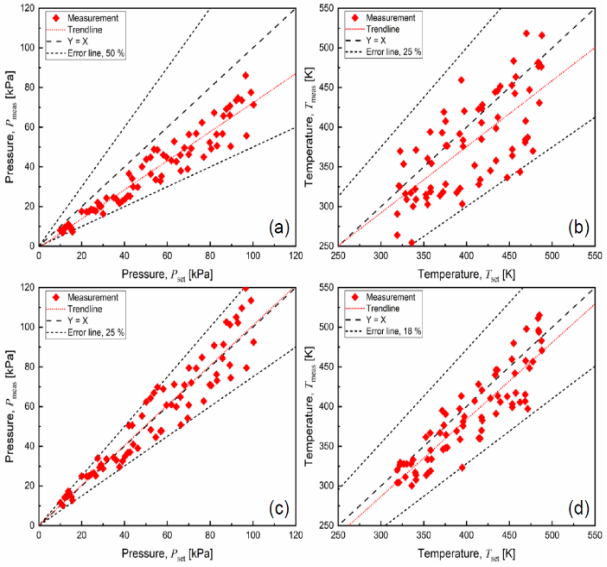

Fig. 13. Comparison between the measured gas property and the set gas property for the test conditions: (a) gas pressure without absorption line recovery; (b) gas temperature without absorption line recovery; (c) gas pressure with absorption line recovery; (d) gas temperature with absorption line recovery [39].

gas property measurement accuracy between the simulation and the experiment is a potential distortion source that could be contained in the measured spectral signal such as optical fringes or non-constant spectral sensitivity of the optical parts. Considering the experimental results for the gas property measurement accuracy, the wing level threshold is determined to be 10 %.

5.4 Gas pressure and temperature measurement

Fig. 12 shows comparisons between the recovered absorbance $A_{meas,recov}(v)$ and the actual absorbance $A_{actual}(v)$ computed from the set gas properties using Eq. (11) for the four test conditions. The residual absorbance between the recovered absorbance and the actual absorbance is shown at the bottom of each individual figure. The four test conditions represent the corner conditions within the target gas property region: (a) relatively low pressure and high temperature, (b) relatively high pressure and temperature, (c) relatively low pressure and temperature, and (d) relatively high pressure and low temperature. By comparing the high-pressure conditions shown in Figs. 12(b) and (d) and the low-pressure conditions shown in Figs. 12(a) and (c), the spectral absorbance at the wing region is higher in the high-pressure conditions. The results shown in Fig. 12 support that the proposed single-line absorption spectroscopy method could successfully recover the measured absorption line for the gas conditions within the target gas property region.

Fig. 13 shows a comparison between the measured gas pressure and temperature with the set gas pressure and temperature for the test conditions. Figs. 13(a) and (b) show the gas pressure and temperature measurement results, respectively, when the absorption line recovery process in steps (g) to (k) is not performed during the single-line absorption spectroscopy method so that the measured absorbance $A_{meas}(v)$ is directly fitted with the calculated absorbance $A_{calc}(v)$. Figs. 13(c) and (d) show the gas pressure and temperature measurement results, respectively, using the proposed single-line absorption spectroscopy method. The Y = X line on which the measurement point is placed when the measured gas property matches the set gas property is shown in Fig. 13. In each graph of Fig. 13, a linear trend line showing the trend of the measured gas properties compared with the set gas properties, and error lines covering all test conditions, is shown.

As shown in Fig. 13, the gas pressure is underestimated by 27 % when the absorption line recovery is not applied so that the calculated absorbance is a direct fit to the measured absorbance. The underestimation of the gas pressure could be caused by the insufficient consideration of collisional broadening in the line-fitting process due to the absorbance loss in the wing region through baseline subtraction. In addition, the measured temperatures have a larger deviation from the set temperature when absorption line recovery is not performed as shown in Fig. 13(b). However, if absorption line recovery is conducted, the gas pressure can be measured without bias and the gas temperature can be measured with lower deviation. By comparing the measured gas properties and the set gas properties, the proposed single-line absorption spectroscopy method could measure the gas pressure and temperature within errors of 25 % and 18 %, respectively.

Fig. 14 shows the gas temperature measurement results for the test conditions when the gas pressure is fixed to the set gas pressure to simulate a situation in which the gas pressure is predetermined using an additional pressure sensor. To

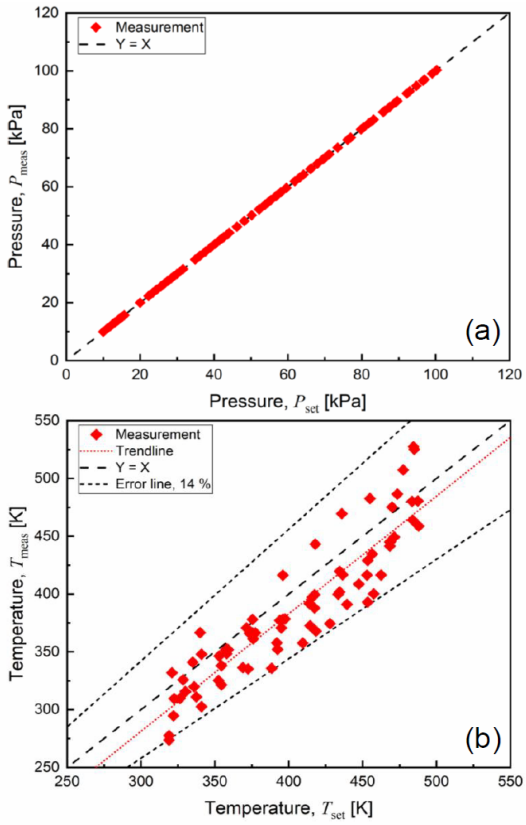

Fig. 14. Comparison between the measured gas temperatures and the set gas temperature for the test conditions under fixed pressure input in the proposed single-line absorption spectroscopy method [39].

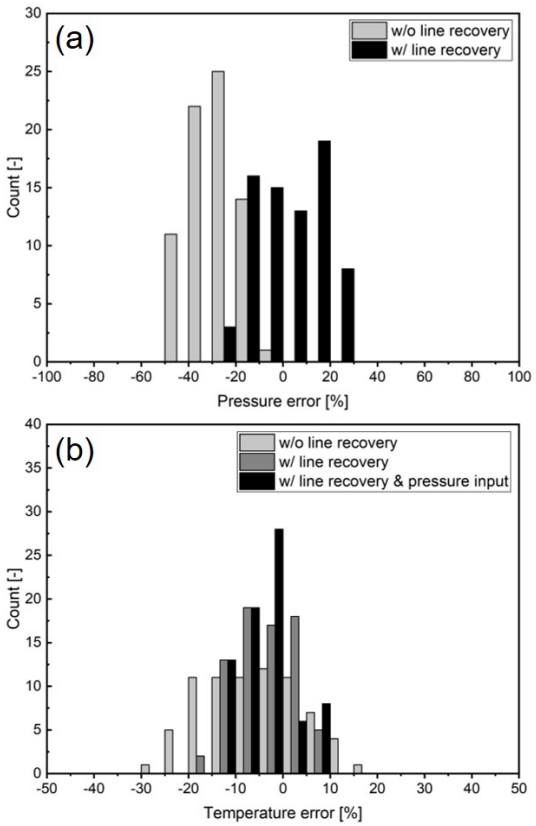

Fig. 15. Measurement error distribution with and without using the proposed single line absorption spectroscopy method for (a) the gas pressure; (b) temperature.

measure the gas temperature, the iteration procedure of the proposed single-line absorption spectroscopy method is conducted by changing the gas temperature while the gas pressure is fixed to the set pressure. Given that the measured gas pressure is the same as the set gas pressure for all test conditions, all measurement points in Fig. 14(a) are placed on the Y = X line. As shown in Fig. 14(b), the gas temperature could be determined within an error of 14% if the gas pressure is predetermined. The gas temperature measurement results suggest that the gas temperature measurement accuracy could be improved if the gas pressure can be determined in advance when using the single-line absorption spectroscopy method.

Fig. 15 shows the comparison between error distributions of gas property measurement with and without applying the proposed spectroscopy method. Figs. 15(a) and (b) represent the measurement error distribution for gas pressure and temperature, respectively. As shown in Fig. 15, all distributions are observed to have a bell shape. However, the mean values and variances are varied with respect to the application of the proposed method. For the gas pressure, the mean value of the error moves towards zero when the proposed method is applied, while the variance is slightly increased. For the gas temperature, the mean value moves to zero and the variance is decreased when the proposed method is applied. When the proposed method and the fixed pressure input are applied, the error distribution is observed to be narrower; the variance is decreased and kurtosis is increased. The error distribution results shown in Fig. 15 imply that the measurement accuracy for pressure and temperature can be increased by using the presented method, with only a minor loss of the pressure variance.

From the experimental gas property measurement results for the test conditions, it is confirmed that the gas pressure and temperature could be simultaneously measured within 25 % and 18 %, respectively, using the proposed method. The measured MAPE values for gas pressure and temperature are 15 % and 5.7 %, respectively. Compared to the similar work by Benoy et al. [12], which measures the gas temperature with a standard deviation of 5 %, the proposed method is observed to have similar accuracy to the traditional method. The proposed single-line absorption spectroscopy method can be used to measure multiple gas properties for gas conditions where only one absorption line can be used within a spectral modulation range of a tunable laser or for space-restricted situations where a limited number of hardware components can be installed.

6. Conclusions

A single-line absorption spectroscopy method is presented for simultaneous measurement of gas pressure and tempera-

ture using a single absorption line. The proposed single-line absorption spectroscopy method can be used to predict the absorbance loss that could occur due to the baseline subtraction to recover the measured absorption line and simultaneously determine the gas pressure and temperature by comparing the recovered absorbance with a calculated absorbance. To predict the absorbance loss, baseline subtraction is also conducted for the calculated absorption line. The concept of the wing level threshold is used to determine the wing region during baseline subtraction. To verify the proposed single-line absorption spectroscopy method, test gas conditions with a pressure range of approximately 10-100 kPa and temperature range of approximately 300-500 K are created in a gas chamber and gas property measurement for the test conditions is performed. Air is used as the test gas and an absorption line of oxygen molecules at a wavenumber of 13150.2 cm^{-1} is used to detect oxygen gas. To verify the proposed single-line absorption spectroscopy method, the gas pressure and temperature for the test conditions are measured using the single-line absorption spectroscopy method and compared with the set gas properties measured using a Bourdon pressure gauge and thermocouples.

From the gas pressure and temperature measurement results for the test conditions, the proposed single-line absorption spectroscopy method can simultaneously measure gas pressure and temperature within errors of 25 % and 18 %, respectively, when the wing level threshold is set to 10 %. In addition, the gas temperature can be measured within an error of 14 % when the gas pressure is predetermined using an additional pressure gauge. The proposed single-line absorption spectroscopy method could be used for simultaneous measurement of gas pressure and temperature when the test gas conditions only allow for a single absorption line to be measured or when space constraints limit the number of laser or optical parts.

Acknowledgments

This work was supported by the Agency for Defense Development by Korean government (No. UC190056CD).

References

[1] D. T. Cassidy and J. Reid, Atmospheric pressure monitoring of trace gases using tunable diode lasers, *Applied Optics*, 21 (7) (1982) 1185-1190.

[2] L. Dong, F. K. Tittel, C. Li, N. P. Sanchez, H. Wu, C. Zheng, Y. Yu, A. Sampaolo and R. J. Griffin, Compact TDLAS based sensor design using interband cascade lasers for mid-IR trace gas sensing, *Optics Express*, 24 (6) (2016) A528.

[3] C. Li, L. Shao, H. Meng, J. Wei, X. Qiu, Q. He, W. Ma, L. Deng and Y. Chen, High-speed multi-pass tunable diode laser absorption spectrometer based on frequency-modulation spectroscopy, *Optics Express*, 26 (22) (2018) 29330.

[4] D. W. Choi, D. H. Doh and M. G. Jeon, The development of the simultaneous reconstruction of 2D temperature and concentration using a 6-peaks algorithm for CT-TDLAS, *Journal of Mechanical Science and Technology*, 34 (5) (2020) 2067-2074.

[5] G. R. Cho and D. W. Choi, Measurement enhancement of TDLAS based on variable weighted cross-correlation tomography for the simultaneous reconstruction of 2D temperature and concentration, *Journal of Mechanical Science and Technology*, 35 (2) (2021) 525-534.

[6] J. Lee, C. Bong, J. Yoo and M. S. Bak, Combined use of TDLAS and LIBS for reconstruction of temperature and concentration fields, *Optics Express*, 28 (14) (2020) 21121.

[7] K. Sun, R. Sur, X. Chao, J. B. Jeffries, R. K. Hanson, R. J. Pummill and K. J. Whitty, TDL absorption sensors for gas temperature and concentrations in a high-pressure entrained-flow coal gasifier, *Proceedings of the Combustion Institute*, 34 (2) (2013) 3593-3601.

[8] R. Sur, K. Sun, J. B. Jeffries, J. G. Socha and R. K. Hanson, Scanned-wavelength-modulation-spectroscopy sensor for CO, CO_2, CH_4 and H_2O in a high-pressure engineering-scale transport-reactor coal gasifier, *Fuel*, 150 (2015) 102-111.

[9] O. Witzel, A. Klein, S. Wagner, C. Meffert, C. Schulz and V. Ebert, High-speed tunable diode laser absorption spectroscopy for sampling-free in-cylinder water vapor concentration measurements in an optical IC engine, *Applied Physics B*, 109 (2012) 521-532.

[10] M. G. Allen, Diode laser absorption sensors for gas-dynamic and combustion flows, *Measurement Science and Technology*, 9 (4) (1998) 545-562.

[11] D. W. Mattison, J. T. C. Liu, J. B. Jeffries, R. K. Hanson, C. M. Brophy and J. O. Sinibaldi, Tunable diodelaser temperature sensor for evaluation of a valveless pulse detonation engine, *Proc. of 43rd AIAA Aerospace Sciences Meeting and Exhibit*, Reno (2005) AIAA 2005-224.

[12] T. Benoy, D. Wilson, M. Lengden, I. Armstrong, G. Stewart and W. Johnstone, Measurement of CO_2 concentration and temperature in an aero engine exhaust plume using wavelength modulation spectroscopy, *IEEE Sensors Journal*, 17 (19) (2017) 6409-6417.

[13] J. Kurtz, S. Wittig and S. O'Byrne, Applicability of a counter-propagating laser airspeed sensor to aircraft flight regimes, *Journal of Aircraft*, 53 (2) (2016) 439-450.

[14] M. S. Brown, G. C. Herring, K. Cabell, N. Hass, T. F. Barhorst and M. Gruber, Optical measurements at the combustor exit of the HIFiRE 2 ground test engine, *Proc. of the 50th AIAA Aerospace Sciences Meeting including the New Horizons Forum and Aerospace Exposition*, Nashville (2012) AIAA 2012-0857.

[15] I. A. Schultz, C. S. Goldenstein, J. B. Jeffries, R. K. Hanson, R. D. Rockwell and C. P. Goyne, Spatially resolved water measurements in a scramjet combustor using diode laser absorption, *Journal of Propulsion and Power*, 30 (6) (2014) 1551-1558.

[16] J. Kurtz, M. Aizengendler, Y. Krishna, P. Walsh, M. Brown and S. O'Byrne, Subsonic in-flight temperature and pressure measurements using a scramjet inlet flow sensor, *AIAA Journal*, 54 (3) (2016) 1007-1013.

[17] S. T. Sanders, J. Wang, J. B. Jeffries and R. K. Hanson, Di-

ode-laser absorption sensor for line-of-sight gas temperature distributions, *Applied Optics*, 40 (24) (2001) 4404-4415.

[18] R. K. Hanson, R. M. Spearrin and C. S. Goldenstein, *Spectroscopy and Optical Diagnostics for Gases*, 1st Ed., Springer, New York (2015).

[19] S. D. Wehe, D. S. Baer and R. K. Hanson, Tunable diode-laser absorption measurements of temperature, velocity, and H_2O in hypervelocity flows, *Proc. of the 33rd Joint Propulsion Conference and Exhibit* (1997) AIAA 97-3267.

[20] A. Farooq, J. B. Jeffries and R. K. Hanson, CO_2 concentration and temperature sensor for combustion gases using diode-laser absorption near 2.7 μm, *Applied Physics B*, 90 (2008) 619-628.

[21] M. E. Webber, J. Wang, S. T. Sanders, D. S. Baer and R. K. Hanson, In situ combustion measurements of CO, CO_2, H_2O and temperature using diode laser absorption sensors, *Proceedings of the Combustion Institute*, 28 (1) (2000) 407-413.

[22] M. P. Arroyo and R. K. Hanson, Absorption measurements of water-vapor concentration, temperature, and line-shape parameters using a tunable InGaAsP diode laser, *Applied Optics*, 32 (30) (1993) 6104-6116.

[23] A. Farooq, J. B. Jeffries and R. K. Hanson, In situ combustion measurements of H_2O and temperature near 2.5 μm using tunable diode laser absorption, *Measurement Science and Technology*, 19 (7) (2008) 075604.

[24] R. Verma, S. Neethu, S. S. Kamble, J. K. Radhakrishnan, P. P. Krishnapur and V. C. Padki, Tunable diode laser absorption spectroscopy based oxygen sensor, *Proc. of the 2012 Sixth International Conference on Sensing Technology* (2012) 130-135.

[25] S. So, D. G. Park, N. Jeong, D. Kim, J. Hwang and C. Lee, Study on the simultaneous measurement of O_2 and CO concentrations in the exhaust gas of a methane/air flame using tunable diode laser absorption spectroscopy, *Energy and Fuels*, 34 (3) (2020) 3780-3787.

[26] C. S. Goldenstein, R. M. Spearrin, I. A. Schultz, J. B. Jeffries and R. K. Hanson, Wavelength-modulation spectroscopy near 1.4 μm for measurements of H_2O and temperature in high-pressure and –temperature gases, *Measurement Science and Technology*, 25 (5) (2014) 055101.

[27] J. T. C. Liu, J. B. Jeffries and R. K. Hanson, Wavelength modulation absorption spectroscopy with 2f detection using multiplexed diode lasers for rapid temperature measurements in gaseous flow, *Applied Physics B*, 78 (2004) 503-511.

[28] C. S. Goldenstein, I. A. Schultz, J. B. Jeffries and R. K. Hanson, Tunable diode laser absorption sensor for measurements of temperature and water concentration in supersonic flows, *Proc. of the 49th AIAA Aerospace Sciences Meeting including the New Horizons Forum and Aerospace Exposition*, Orlando (2011) AIAA 2011-1094.

[29] J. T. C. Liu, G. B. Rieker, J. B. Jeffries, M. R. Gruber, C. D. Carter, T. Mathur and R. K. Hanson, Near-infrared diode laser absorption diagnostic for temperature and water vapor in a scramjet combustor, *Applied Optics*, 44 (31) (2005) 6701-6711.

[30] R. M. Spearrin, W. Ren, J. B. Jeffries and R. K. Hanson, Multi-band infrared CO_2 absorption sensor for sensitive temperature and species measurements in high-temperature gases, *Applied Physics B*, 116 (2014) 855-865.

[31] M. E. Webber, S. Kim, S. T. Sanders, D. S. Baer, R. K. Hanson and Y. Ikeda, In situ combustion measurements of CO_2 by use of a distributed-feedback diode-laser sensor near 2.0 μm, *Applied Optics*, 40 (6) (2001) 821-828.

[32] S. J. Chen, M. E. Paige, J. A. Silver, S. Williams and T. Barhorst, Laser-based mass flow rate sensor onboard HIFiRE flight 1, *Proc. of the 45th AIAA/ASME/SAE/ASEE Joint Propulsion Conference and Exhibit*, Denver (2009) AIAA 2009-5065.

[33] A. Sappey, P. McCormick, P. Masterson, Q. Zhao, L. Sutherland, I. Smith, P. VanHoudt, J. Hannam, D. Owenby, S. Williams and T. Barhorst, Development of a flight-worthy tdlas-based oxygen sensor for HIFiRE-1, *Proc. of the 45th AIAA/ASME/SAE/ASEE Joint Propulsion Conference and Exhibit*, Denver (2009) AIAA 2009-4971.

[34] T. Barhorst, S. Williams, S. J. Chen, M. E. Paige, J. A. Silver, A. Sappey, P. McCormick, P. Masterson, Q. Zhao, L. Sutherland, I. Smith, P. VanHoudt, J. Hannam and D. Owenby, Development of an in flight nonintrusive mass capture system, *Proc. of the 45th AIAA/ASME/SAE/ASEE Joint Propulsion Conference and Exhibit*, Denver (2009) AIAA 2009-5067.

[35] M. S. Brown and T. F. Barhorst, Post-flight analysis of the diode-laser-based mass capture experiment onboard HIFiRE flight 1, *Proc. of the 17th AIAA International Space Planes and Hypersonic Systems and Technologies Conference*, San Francisco (2011) AIAA 2011-2359.

[36] S. O'Byrne, S. Wittig, J. Kurtz, Y. Krishna, C. Rodriguez, M. Aizengendler and J. Davies, *Diode Laser Sensor for Scramjet Inlets: Final Year Report*, US Airforce Office of Aerospace Research and Development (2011).

[37] C. S. Goldenstein, R. M. Spearrin, J. B. Jeffries and R. K. Hanson, Infrared laser-absorption sensing for combustion gases, *Progress in Energy and Combustion Science*, 60 (2016) 132-176.

[38] H. Shim, S. Jung, G. Kim and G. Park, Air density measurement in a narrow test section using a laser absorption spectroscopy, *Journal of the Korean Society for Aeronautical and Space Sciences*, 49 (11) (2021) 893-900.

[39] H. Shim, Design of a laser absorption spectroscopy based compact gas analyzing sensor for high speed flow diagnosis, *Ph.D. Thesis*, Korea Advanced Institute of Science and Technology, Republic of Korea (2022).

[40] Y. Krishna, S. O'Byrne and J. J. Kurtz, Baseline correction for stray light in log-ratio diode laser absorption measurements, *Applied Optics*, 53 (19) (2014) 4128-4135.

[41] J. Kurtz, M. Aizengendler, Y. Krishna, P. Walsh and S. O'Byrne, Rugged, scramjet inlet temperature and velocity sensor: design and ground test, *AIAA Journal*, 54 (2) (2016) 1-9.

[42] B. J. Wheatley, Applications of tunable diode laser absorption spectroscopy to aerospace flows, *Ph.D. Thesis*, University of Queensland, Australia (2017).

[43] V. Weldon, J. O'Gorman, J. J. Pérez-Camacho, D. McDonald, J. Hegarty, J. C. Connolly, N. A. Morris, R. U. Martinelli and J. H. Abeles, Laser diode based oxygen sensing: a comparison of VCSEL and DFB laser diodes emitting in the 762 nm region,

Infrared Physics and Technology, 38 (6) (1997) 325-329.
[44] K. M. Busa, Development of tunable diode laser absorption tomography and application to scramjet engines, *Ph.D. Thesis*, University of Virginia, USA (2014).
[45] A. Lytkine, W. Jaeger and J. Tulop, Long-wavelength vcsels for applications in absorption spectroscopy: tuning rates and modulation performances, *Proceedings of SPIE*, San Jose (2005).
[46] L. C. Philippe and R. K. Hanson, Laser diode wavelength-modulation spectroscopy for simultaneous measurement of temperature, pressure, and velocity in shock-heated oxygen flows, *Applied Optics*, 32 (30) (1993) 6090-6103.
[47] X. Liu, J. B. Jeffries and R. K. Hanson, Measurements of spectral parameters of water-vapour transitions near 1388 and 1345 nm for accurate simulation of high-pressure absorption spectra, *Measurement Science and Technology*, 18 (2007) 1185-1194.
[48] S. Schilt and L. Thévenaz, Experimental method based on wavelength-modulation spectroscopy for the characterization of semiconductor lasers under direct modulation, *Applied Optics*, 43 (22) (2004) 4446-4453.
[49] J. Skrotzki, J. C. Habig and V. Ebert, Integrative fitting of absorption line profiles with high accuracy, robustness, and speed, *Applied Physics B*, 116 (2014) 393-406.
[50] J. Li, B. Yu and H. Fischer, Wavelet transform based on the optimal wavelet pairs for tunable diode laser absorption spectroscopy signal processing, *Applied Spectroscopy*, 69 (4) (2015) 496-506.
[51] J. M. Weisberger, J. P. Richter, R. A. Parker and P. E. DesJardin, Direct absorption spectroscopy baseline fitting for blended absorption features, *Applied Optics*, 57 (30) (2018) 9086-9095.
[52] I. E. Gordon, L. S. Rothman, C. Hill, R. V. Kochanov, Y. Tan, P. F. Bernath, M. Birk, V. Boudon, A. Campargue, K. V. Chance, B. J. Drouin, J. M. Flaud, R. R. Gamache, J. T. Hodges, D. Jacquemart, V. I. Perevalov, A. Perrin, K. P. Shine, M. A. H. Smith, J. Tennyson, G. C. Toon, H. Tran, V. G. Tyuterev, A. Barbe, A. G. Császár, V. M. Devi, T. Furtenbacher, J. J. Harrison, J. M. Hartmann, A. Jolly, T. J. Johnson, T. Karman, I. Kleiner, A. A. Kyuberis, J. Loos, O. M. Lyulin, S. T. Massie, S. N. Mikhailenko, N. Moazzen-Ahmadi, H. S. P.Müller, O. V. Naumenko, A. V. Nikitin, O. L. Polyansky, M. Rey, M. Rotger, S. W. Sharpe, K. Sung, E. Starikova, S. A. Tashkun, J. V. Auwera, G. Wagner, J. Wilzewski, P. Wcisło, S. Yu and E. J. Zak, The HITRAN2016 molecular spectroscopic database, *Journal of Quantitative Spectroscopy and Radiative Transfer*, 203 (2017) 3-69.
[53] S. M. Abrarov and B. M. Quine, Efficient algorithmic implementation of the Voigt/complex error functionbased on exponential series approximation, *Applied Mathematics and Computation*, 218 (2011) 1894-1902.
[54] K. J. Ritter and T. D. Wilkerson, High-resolution spectroscopy of the oxygen A band, *Journal of Molecular Spectroscopy*, 121 (1) (1987) 1-19.
[55] L. R. Brown and C. Plymate, Experimental line parameters of the oxygen A band at 760 nm, *Journal of Molecular Spectroscopy*, 199 (2) (2000) 166-179.

Hanseul Shim received his Ph.D. in 2022 from the KAIST, Daejeon, Republic of Korea. He is currently a Postdoctoral Research Associate of the Department of Mechanical Science and Engineering of the University of Illinois at Urbana-Champaign. His research interests include optical flow diagnostics, hypersonic flow, and propulsion.

Gyeongrok Kim received his Master's degree in 2018 from the KAIST, Daejeon, Republic of Korea. He is currently a Ph.D. candidate of the Department of Aerospace Engineering of KAIST. His research interests include hypersonic flows, flow diagnostics, thermal stress-based material failure, and thermal protection systems.

Sion Jung received his Master's degree in 2022 from the KAIST, Daejeon, Republic of Korea. He is currently a Ph.D. candidate of the Department of Aerospace Engineering of KAIST. His research interests include hypersonic flows, flow diagnostics, and laser absorption spectroscopy.

Gisu Park received his Ph.D. in 2010 from University of New South Wales. He is currently an Associate Professor of the Department of Aerospace Engineering of KAIST, Daejeon, Republic of Korea. His research interests include hypersonic aerothermodynamics and high-speed ground tests.